https://doi.org/10.5194/egusphere-2026-4310
Preprint. Discussion started: 28 July 2026

GlaDS-2: modeling subglacial drainage including ice uplift and free-surface flow in two dimensions

Sandra Wells[1,2], Ivan Utkin[1,2], Ian J. Hewitt[3], Daniel Farinotti[1,2], and Mauro A. Werder[1,2]

[1]Laboratory of Hydraulics, Hydrology and Glaciology (VAW), ETH Zurich, Zurich, Switzerland
[2]Swiss Federal Institute for Forest, Snow and Landscape Research (WSL), Birmensdorf, Switzerland
[3]Mathematical Institute, University of Oxford, Oxford, UK

Correspondence: Sandra Wells (swells@ethz.ch)

Abstract. Subglacial drainage is a crucial component of the dynamics of glaciers and ice sheets, through its impact on basal sliding, ice flow velocities, and ultimately, glacier mass loss. Numerical models of subglacial drainage that combine both distributed and channelized flow in 2D have enabled many studies of subglacial hydrology and its link to ice flow. However, existing 2D models are fundamentally limited by their inability to incorporate the physical representation of ice uplift, when water pressure reaches ice overburden, and free-surface flow at atmospheric pressure. We present GlaDS-2, a new subglacial drainage model that addresses this modeling gap by incorporating bounded subglacial water pressures into a novel, unified, and mass-conserving formulation. GlaDS-2 builds upon the Glacier Drainage System (GlaDS) model by including physics-based representations of ice uplift and free-surface flow in addition to pressurized subglacial flow, and implicitly captures the evolving boundaries between different flow regimes. We showcase the new capabilities of the model by simulating a rapid supraglacial lake drainage on both synthetic and real topography from North Lake in Greenland. The model simulates the formation and dissipation of a traveling subglacial water blister inducing transient ice uplift, captures regions of free-surface flow at the ice margins, and integrates the modeling of proglacial flow dynamics. Our simulations demonstrate that the spatial and temporal extent of the ice uplift following the lake drainage is influenced by both englacial storage and the pre-existing state of the subglacial channel network. Overall, GlaDS-2 provides an improved numerical foundation for future coupled subglacial drainage and ice-flow modeling.

1 Introduction

The subglacial drainage system is a key driver of transient fluctuations in basal sliding and, thus, of ice-sheet and glacier flow. Changes in this system can be driven, for example, by internal drainage dynamics (e.g. Stearns et al., 2008), climate-driven variations in surface meltwater input (e.g. Sundal et al., 2011), episodic lake drainages (e.g. Maier et al., 2023), or glacier retreat (e.g. Zhao et al., 2025). Understanding these dynamic relationships therefore requires comprehensive modeling of subglacial processes. To this end, numerical models of subglacial drainage have evolved to simulate water flow in two dimensions at the ice-bed interface and generally feature both distributed and channelized drainage, often based on linked cavities (Walder, 1986; Kamb, 1987; Hewitt, 2011) for the former and ice-incised R-channels (Röthlisberger, 1972; Nye, 1976) for the latter. In their implementation, these models either are physics based (e.g. Schoof, 2010; Hewitt, 2013; Werder et al., 2013; Bueler and van

https://doi.org/10.5194/egusphere-2026-4310
Preprint. Discussion started: 28 July 2026

Pelt, 2015; Sommers et al., 2018; Felden et al., 2023), emulate physics-based models (e.g., Verjans and Robel, 2024), or are based on parameterizations (e.g., de Fleurian et al., 2014; Beyer et al., 2018; Kazmierczak et al., 2024).

The Glacier Drainage System (GlaDS) model (Werder et al., 2013) is one of the most widely used physics-based subglacial drainage models that incorporates distributed and channelized flow. In the classification of Flowers (2015), GlaDS is a latest-generation, physically-based, two-dimensional, multi-element model. It has been implemented and used in its original MATLAB version (e.g., Dow et al., 2016; Hill et al., 2023), within the ice flow model Elmer/Ice (e.g., Gagliardini and Werder, 2018; Scholzen et al., 2021; Cook et al., 2022), within the ice flow model ISSM (e.g., Ehrenfeucht et al., 2023; McArthur et al., 2023), and in other independent codes (e.g., Downs et al., 2018; Brinkerhoff et al., 2021).

Previous two-dimensional models, including GlaDS, neglect ice uplift caused by hydraulic jacking and fail to capture free-surface flow by restricting the subglacial space to a permanently water-filled state. The reason for these two omissions is that their thus far proposed implementations are non-trivial from both a mathematical and numerical point of view. However, ice uplift is often observed during the rapid drainage of supraglacial lakes (e.g. Das et al., 2008), above subglacial lakes (e.g. Gray et al., 2005), during spring events before the efficient summer drainage system is developed (e.g. Iken et al., 1983), in glacier surges (e.g. Kamb and Engelhardt, 1987), and in jökulhlaups (e.g. Huss et al., 2007), among others. Likewise, free-surface flow is often present on steep slopes and near land-terminating ice sheet outlet glaciers and glacier termini (e.g. Nienow et al., 1996). Properly incorporating all three subglacial water pressure regimes would improve the physical accuracy of subglacial drainage modeling in many scenarios. In the bigger picture, this improvement holds direct relevance to ice flow modeling through the well-established impact of effective pressure on ice sliding speed and, thus, ice-sheet-driven sea-level rise (e.g., Schoof, 2010; Stevens et al., 2018; Maier et al., 2023; Zhao et al., 2025).

Small-scale models that take into account ice uplift have been proposed, such as elastic models for the rapid drainage of surface lakes in Greenland (e.g., Tsai and Rice, 2010; Lai et al., 2021). Ice uplift and free-surface flow directly incorporated into GlaDS or another latest-generation hydrology model is thus far limited to two companion papers (Schoof et al., 2012; Hewitt et al., 2012), but their numerical implementation was restricted to one dimension. Their approach is computationally demanding due to the three different physical regimes solving different model equations, and their domain boundaries needing careful tracking and enforcement of mass conservation. Therefore, a crucial next step for future studies is to scale these implementations into two dimensions and enhance their numerical performance.

A recent study by Zhang et al. (2025) developed a model for subglacial blisters as a viscous water flow component under an elastic ice sheet, connected to a two-dimensional subglacial drainage model through a leakage term. This approach can effectively incorporate the ice uplift behavior associated with subglacial blisters in two dimensions, but it remains restricted to the modeling of blisters resulting from supraglacial lake drainage events, and does not incorporate free-surface flow.

In this work, we introduce GlaDS-2, a new subglacial drainage model that builds upon GlaDS and includes ice uplift, pressurized flow, and free-surface flow regimes in two dimensions. Our implementation is based on a bounded equation for the water pressure, and a mass-conserving approach that does not require the boundaries between regime domains to be tracked; they can instead be obtained by post-processing. The spatial grids and numerical solver are designed to be compatible with GPU computing, which will enable large-scale, high-resolution simulations in future work.

https://doi.org/10.5194/egusphere-2026-4310
Preprint. Discussion started: 28 July 2026

The paper is structured as follows. In Sect. 2, we introduce the physics and numerical approach implemented in GlaDS-2. In Sect. 3, we compare the results of our model to those of Schoof et al. (2012) and Hewitt et al. (2012). In Sect. 4, we use GlaDS-2 to simulate a rapid supraglacial lake drainage on synthetic topography (Sect. 4.1) and on real topography (Sect. 4.2). In Sect. 5 and Sect. 6, we discuss our results, show avenues for future work, and present concluding remarks.

2 Methods

GlaDS-2 simulates subglacial water flow through both the distributed and channelized drainage system. The former system is modeled with subglacial sheet equations (Sect. 2.1), and the latter with R-channel equations (Sect. 2.2). The model runs on a two-dimensional domain $(x,\, y) \in \Omega$ with boundary $\delta\Omega$, on which bed elevation $B = B(x,\, y)$ and ice thickness $H = H(x,\, y)$ are defined. The model requires initial conditions of the subglacial drainage system, boundary conditions on $\delta\Omega$, and a definition of the water input m on Ω. The variables and parameters used in the model are listed in Table 1 and 2, respectively.

The approach in GlaDS-2 builds upon the physics for the subglacial sheet and channels in GlaDS (Werder et al., 2013), uses a structured grid comparable to Hewitt (2013), and incorporates the subglacial regimes of ice uplift and free-surface flow as in Schoof et al. (2012) and Hewitt et al. (2012). Similar to Bueler and van Pelt (2015), our approach is mass-conserving and uses a closure relation that defines water pressure as a function of the amount of water.

When including the physical regimes of ice uplift and free surface flow, the regions on which these occur are themselves part of the solution. This poses a free-boundary problem, which was previously solved through variational inequalities (Schoof et al., 2012). We instead implement a front-capturing approach, solving a single set of equations for all three regions and using a piecewise closure relation connecting system variables, which we detail in Sect. 2.1.

To model ice uplift without coupling to an ice-flow model, we assume hydrostatic ice overburden pressure and static ice thickness. Consequently, ice uplift is represented as occurring instantaneously once subglacial water pressure equals ice overburden pressure. The implications of these simplifying assumptions are discussed in detail in Sect. 5.3.

Including free-surface flow directly extends our modeling approach to the proglacial zone (where the ice thickness is zero). Fundamentally, representing flow at atmospheric pressure allows the same governing equations to be solved in both unpressurized subglacial space and unglaciated regions, enabling a continuous transition between subglacial and proglacial water flow.

2.1 Subglacial sheet equations

We describe the distributed drainage system together with the englacial system and define h to be the total volume of water per unit area of the bed (the water can be anywhere within the ice column, see Fig. 1a). This is partitioned into the flowing thickness h_w, and a thickness of stored water, h_e:

$$h = h_w + h_e. \tag{1}$$

https://doi.org/10.5194/egusphere-2026-4310
Preprint. Discussion started: 28 July 2026

Table 1. Variables of the model and their units.

Description	Symbol	Units
Time	t	s
Horizontal coordinates	x, y	m
Along channel coordinate	s	m
Sheet water height	h	m
Flowing sheet thickness	h_w	m
Stored water thickness	h_e	m
Mean cavity height	h_g	m
Storage capacity thickness	Δh	m
Water pressure	p_w	Pa
Hydraulic potential	ϕ	Pa
Effective pressure	N	Pa
Sheet water flux	$\mathbf{q}$	$\mathrm{m^2\,s^{-1}}$
Sheet flux along channel	q_c	$\mathrm{m^2\,s^{-1}}$
Melt input	m	$\mathrm{m\,s^{-1}}$
Channel cross-section	S	$\mathrm{m^2}$
Water-filled channel cross-section	S_w	$\mathrm{m^2}$
Channel radius	R	m
Water-filled channel height	R_w	m
Channel discharge	Q	$\mathrm{m^3\,s^{-1}}$
Dissipation power	Ξ	$\mathrm{W\,m^{-1}}$
Pressure-melting power	Π	$\mathrm{W\,m^{-1}}$
Effective diffusivity	D_{eff}	$\mathrm{m^2\,s^{-1}}$
Effective velocity	$\mathbf{V}_{\mathrm{eff}}$	$\mathrm{m\,s^{-1}}$

When the flow is pressurized, as assumed in the original GlaDS model, the flowing thickness h_w is equal to the locally-averaged cavity height h_g, the evolution of which we discuss below. But under conditions of ice uplift we now allow $h_w > h_g$, and under free-surface flow we have $h_w < h_g$, as illustrated in Fig. 1a. Note that our notation is slightly different from that used in the original GlaDS model, where h was used to mean h_w here, and only the pressurized case was considered.

The stored component h_e is most easily thought of as englacial storage, which is assumed to be proportional to the basal water pressure p_w,

$$h_e = e_v \frac{p_w}{\rho_w g}, \tag{2}$$

where e_v represents the englacial void ratio. However, it is also possible to interpret h_e as other stored water, the volume of which is proportional to water pressure (such a relation might occur due to linear elastic deformation of fractures within the ice,

https://doi.org/10.5194/egusphere-2026-4310
Preprint. Discussion started: 28 July 2026

Table 2. Parameters of the model with their default value and units.

Description	Symbol	Units	Value
Sheet conductivity	k	$\mathrm{m}^{7/4}\,\mathrm{kg}^{-1/2}$	0.01
Channel conductivity	k_c	$\mathrm{m}^{3/2}\,\mathrm{kg}^{-1/2}$	0.1
Flow law area exponent	α	–	$5/4$
Flow law grad. exponent	β	–	$3/2$
Rheol. const. cavities	A	$\mathrm{Pa}^{-n}\,\mathrm{s}^{-1}$	6.75×10^{-24}
Rheol. const. channels	A_c	$\mathrm{Pa}^{-n}\,\mathrm{s}^{-1}$	6.75×10^{-24}
Glen's law exponent	n	–	3
Englacial void ratio	e_v	–	10^{-4} [a]
Cavity spacing	l_r	m	2
Basal sliding speed	u_b	$\mathrm{m\,s}^{-1}$	3.2×10^{-6} [b]
Bump height	h_r	m	0.1
Sheet melt width	l_c	m	2
Clapeyron slope	c_t	$\mathrm{K\,Pa}^{-1}$	-7.5×10^{-8}
Heat capacity of water	c_w	$\mathrm{J\,kg}^{-1}\,\mathrm{K}^{-1}$	4220
Latent heat of fusion	L	$\mathrm{J\,kg}^{-1}$	3.34×10^{5}
Water density	ρ_w	$\mathrm{kg\,m}^{-3}$	1000
Ice density	ρ_i	$\mathrm{kg\,m}^{-3}$	910
Gravitational accel.	g	$\mathrm{m\,s}^{-2}$	9.81
Bed elevation	B	m	
Ice thickness	H	m	
Ice overburden pressure	p_i	Pa	

[a] Except where explicitly modified in Sect. 3 and Sect. 4.1.1
[b] Equivalent to $100\,\mathrm{m\,a}^{-1}$

for example). Similar relationships (though not necessarily linear) have been used by Flowers and Clarke (2002) and Bueler
100 and van Pelt (2015), where they instead assumed storage occurred in porous sediment.

Since we restrict p_w not to exceed the ice-overburden pressure p_i (detailed below), the maximum amount of storage is

$$\Delta h = e_v \frac{p_i}{\rho_w g} = e_v \frac{\rho_i}{\rho_w} H, \tag{3}$$

where H is the ice thickness (here, we take $p_i = \rho_i g H$, though when coupled to a Stokes ice-flow model, it should be replaced by the normal stress σ_{nn} at the bed).

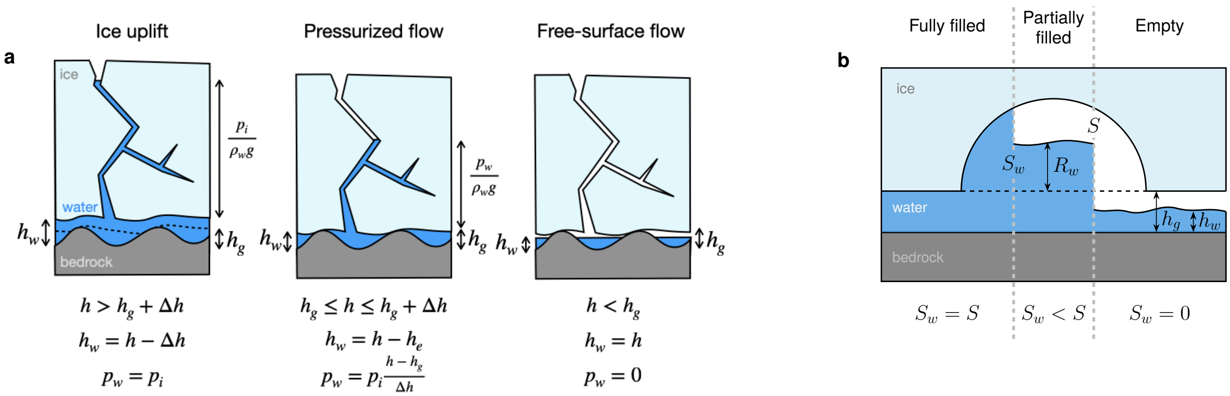

Figure 1. Sketch of the different regimes in the subglacial sheet and channels. (a) Side view of subglacial sheet drainage and englacial storage in ice uplift, pressurized flow, and free-surface flow regimes. (b) Cross-sectional view of an R-channel above the subglacial sheet, in its fully-filled, partially-filled, and empty regimes. Fully-filled channels take place with ice uplift or pressurized flow in the sheet, partially-filled channels with pressurized flow in the sheet, and empty channels with free-surface flow in the sheet.

Considering (1), (2), and (3) allows us to relate the water pressure directly to h through a closure relation that bounds the water pressure between atmospheric and ice overburden pressure:

$$p_w = \begin{cases} p_i & \text{if } \; h > h_g + \Delta h \\ p_i (h - h_g)/\Delta h & \text{if } \; h_g \le h \le h_g + \Delta h \\ 0 & \text{if } \; h < h_g. \end{cases} \tag{4}$$

This is the key component of the model that distinguishes the three physical regimes in the subglacial water sheet:

– Ice uplift: $h > h_g + \Delta h$. Cavities and englacial storage are both completely filled, and additional water entering the sheet is accommodated through hydraulic jacking, with the value of the water pressure staying constant at ice overburden pressure. In this regime, $h_e = \Delta h$ and $h_w = h - h_e$.

– Pressurized flow: $h_g \le h \le h_g + \Delta h$. Cavities are completely filled with water, and additional water entering the sheet is incorporated into englacial storage in an elastic manner, elevating the value of water pressure from atmospheric pressure and up to ice overburden pressure. In this regime, $h_w = h_g$ and $0 \le h_e \le \Delta h$.

– Free-surface flow: $h < h_g$. Water flows through cavities that are partially filled, with the value of water pressure staying constant at atmospheric pressure. In this regime, $h_w = h$ and $h_e = 0$.

Within the proglacial zone, $p_i = 0$ holds true independently of h and h_g (the latter being physically meaningless in this region of the domain). Consequently, the value $p_w = 0$ is enforced on proglacial water flow by design, as the upper and lower pressure boundaries in Eq. (4) collapse to atmospheric pressure.

We have not yet said anything about the average cavity height h_g, which itself can vary in space and time. As detailed in Hewitt (2011) and Werder et al. (2013), this is assumed to evolve through a combination of opening by sliding over bedrock bumps, and closing through creep closure, following the relation

$$\frac{\partial h_g}{\partial t} = \frac{u_b}{l_r}(h_r - h_g) - \frac{2}{n^n} A h_g N^n, \tag{5}$$

where t is time, u_b is the basal sliding speed, l_r the typical horizontal cavity spacing, h_r is the typical bedrock bump height, n is the exponent in Glen's law, A represents the multiplication of the rheological constant of ice times an order-one geometrical factor that depends on the shape of the cavities, and $N = p_i - p_w$ is the effective pressure. In our model, N is always non-negative (a consequence of the definition of the subglacial water pressure in Eq. (4)), so Eq. (5) implicitly ensures that h_g remains bounded between 0 and h_r.

We define the water flux through the distributed sheet $\mathbf{q}$ using the Darcy-Weisbach relation for turbulent flow:

$$\mathbf{q} = -k h_w^{\alpha} |\nabla \phi|^{\beta - 2} \nabla \phi, \tag{6}$$

where k is the sheet conductivity, α and β are the water flow law exponents, and ϕ is the hydraulic potential driving the flow. We define the latter as

$$\phi = \rho_w g (B + h_w) + p_w, \tag{7}$$

where ρ_w is the density of water, g is the gravitational acceleration, B is the bed elevation. Unlike the original GlaDS model (Werder et al., 2013), we retain the influence of the sheet thickness h_w on the depth averaged water pressure (assuming a hydrostatic profile), and are therefore specifically taking p_w to be the water pressure at the top of the flowing part of the sheet.

To help visualise the hydraulic potential in the figures, we also define the bed elevation potential,

$$\phi_m = \rho_w g B, \tag{8}$$

and the overburden hydraulic potential,

$$\phi_0 = \rho_w g B + \rho_i g H. \tag{9}$$

From the bounds on the water pressure we always have $\phi_m \leq \phi - \rho_w g h_w \leq \phi_0$.

2.2 Subglacial channel equations

We include channelized flow on a discrete subset of the two-dimensional domain, defined by the edges of the prescribed numerical mesh. Channels open through melt due to energy dissipation in turbulent flow, and close through viscous creep. The time evolution of a channel's cross-sectional area S follows the equations

$$\frac{\partial S}{\partial t} = \frac{\Xi + \Pi}{\rho_i L} - \frac{2}{n^n} A_c S N^n, \tag{10}$$

$$\Xi = -Q \frac{\partial \phi}{\partial s} - l_c q_c \frac{\partial \phi}{\partial s}, \tag{11}$$

$$\Pi = -c_t c_w \rho_w (Q + f l_c q_c) \frac{\partial p_w}{\partial s}, \tag{12}$$

https://doi.org/10.5194/egusphere-2026-4310
Preprint. Discussion started: 28 July 2026

where Q is the discharge along the channels, Ξ corresponds to the melt originating from the potential energy dissipated by water flow, Π to the melt or freeze from the heat originating from changes to the pressure melting point of the ice on the channel walls (note that our sign convention for both Π and c_t differ from Werder et al. (2013)), A_c is the rheological constant of ice in the channels (as we assume semi-circular channels, no geometrical factor is absorbed into A_c), s is the coordinate along the channel, l_c is a length scale representing the width of the sheet around a channel that contributes to channel melt, q_c the discharge in the sheet along the channel direction, c_t is the Clapeyron slope, c_w is the specific heat capacity of water, and f is a switch to prevent channel size from becoming negative:

$$f = \begin{cases} 1 & \text{if } S > 0 \text{ or } q_c \frac{\partial p_w}{\partial s} > 0, \\ 0 & \text{otherwise.} \end{cases} \tag{13}$$

We allow the water-filled section of the channels S_w to be lower or equal to their total cross-sectional area S. The first case corresponds to partially water-filled channels, and the latter case to fully water-filled ones. To find S_w, we assume that channels have a semicircular area with radius R, thus $S = \pi R^2/2$, and we calculate the water-filled height R_w as

$$R_w = \min\left(\frac{h_e}{e_v},\, R\right) = \min\left(\frac{p_w}{\rho_w g},\, R\right). \tag{14}$$

The water-filled cross-section S_w can then be found using R_w as the circular segment apothem through the relation

$$S_w = \min\left(S - \left(R^2 \arccos\left(\frac{R_w}{R}\right) - R_w\sqrt{R^2 - R_w^2}\right),\, S\right). \tag{15}$$

The different regimes for channel flow are illustrated in Fig. 1b. Each channel regime corresponds to a specific flow regime in the surrounding sheet: fully filled channels co-occur with either ice uplift or pressurized sheet flow, partially filled channels with pressurized sheet flow, and empty channels with free-surface sheet flow.

Discharge in the channels Q follows the turbulent flow law

$$Q = -k_c S_w^{\alpha} \left|\frac{\partial \phi}{\partial s}\right|^{\beta-2} \frac{\partial \phi}{\partial s}, \tag{16}$$

similar to Eq. (6), and where k_c is the conductivity of the channels, and α and β are the same flow law exponents as in Eq. (6). We keep the conductivity k_c constant by assuming in Eq. (16) that S_w is of semi-circular shape. This is a slight simplification with respect to the truncated semi-circular shape of S_w in Eq. (15), see Schuler and Fischer (2009) for a more thorough treatment.

2.3 Combined mass conservation

We assume for simplicity that the volume of the water in the channels is negligible (i.e. they conduct water at a rate Q without themselves providing any storage capacity). Conservation of mass is then expressed as

$$\frac{\partial h}{\partial t} + \nabla \cdot \mathbf{q} + \frac{\partial Q}{\partial s}\delta(\mathbf{x}_c) = m + \frac{\Xi + \Pi}{\rho_w L}\delta(\mathbf{x}_c), \tag{17}$$

https://doi.org/10.5194/egusphere-2026-4310
Preprint. Discussion started: 28 July 2026

where m is the melt input, and the delta function $\delta(\mathbf{x}_c)$ is non-zero at the 1D subset of the domain $\mathbf{x}_c$ on which channels are defined. (If the volume of water stored in the channels were included, an additional small term $\partial S_w/\partial t\, \delta(\mathbf{x}_c)$ would appear on the left hand side of this equation, which could be handled numerically but would add disproportionate complexity to benefit).

Boundary conditions on Eq. (17) can be defined through h or $\mathbf{q}$. This is straightforward for set values of h such as in the case of ocean-terminating glaciers where h at a proglacial boundary remains at sea level, and for set values of $\mathbf{q}$ such as in the case of a known inflow or outflow (including no flow). It is less straightforward for boundary conditions on water pressure. In this case, e.g., in the case of imposing atmospheric pressure at a boundary, we use the ghost-point method and impose h on a point outside of the numerical grid from the condition $p_w = 0$.

2.4 Numerical approach

We use finite differences to discretize the 2D domain. Specifically, we implement a structured, staggered grid, with constant grid spacing $(\Delta x, \Delta y)$ as shown in Fig. 2. Variables h, h_g, and m (and derived variables ϕ, p_w, h_w, h_e, Δh) are defined on the cell centers. The sheet flux components, $\mathbf{q} = (q_x, q_y)$, are defined in a staggered way, on their respective cell edges. Channel discharge Q, as well as channel variables S and S_w (and derived variables R, R_w, Ξ, and Π), are defined on the cell edges.

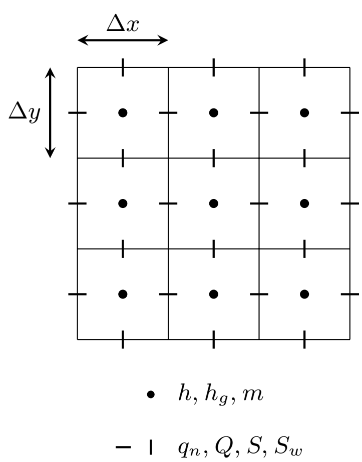

Figure 2. 2D staggered grid showing spatial discretization and variable locations. q_n denotes the normal component of $\mathbf{q}$ on each cell edge, such that $q_n = q_x$ on vertical edges (–) and $q_n = q_y$ on horizontal edges (|).

We solve the mass conservation equation (Eq. (17)) for h as the main partial differential equation (PDE). This differs from the approach in the original GlaDS implementation, which instead solved a PDE for the hydraulic potential ϕ. By solving for the conserved quantity h, and using a conservative numerical method as detailed below, mass conservation is directly ensured. Also notably, the transitions from free-surface flow to pressurized flow, and from pressurized flow to ice uplift, do not need to be tracked and can instead be found in post-processing.

At each time step, our numerical approach executes the following steps:

https://doi.org/10.5194/egusphere-2026-4310
Preprint. Discussion started: 28 July 2026

1. h_w, p_w, ϕ, S_w, $\mathbf{q}$, and Q are computed using the relations (1), (4), (7), (15), (6), and (16), respectively.
2. The time-step size is calculated from the values found in step 1 as detailed in Sect. 2.5.
3. h is updated by integrating PDE (17) for mass conservation, using a forward Euler scheme in time and central differences in space.
4. h_g and S are updated by discretizing the ODEs (5) and (10), respectively, using semi-implicit Euler in time.

2.5 Time-step size calculation

Since we use explicit time integration, the time step must be calculated from stability bounds. We find the approximate values for these bounds by linearizing the equations at each time step, and identifying diffusive and advective components of water flow in Eq. (17). We distinguish these components by finding the values of the effective diffusivity D_{eff} and effective velocity $\mathbf{V}_{\text{eff}}$, such that

$$\mathbf{q}+Q\delta(\mathbf{x}_c)\hat{\mathbf{s}} \approx -D_{\text{eff}}(h,\nabla h)\nabla h+\mathbf{V}_{\text{eff}}(h,\nabla h)h+\mathbf{f}, \tag{18}$$

where $\hat{\mathbf{s}}$ is the unit vector in the direction of channel flow, and $\mathbf{f}$ represents the terms that do not depend on h and ∇h. As $\mathbf{q}$ and Q are nonlinear in h and ∇h, a full decoupling of diffusive and advective terms is not straightforward. D_{eff} and V_{eff} are defined by identification from $\mathbf{q}(h,\nabla h)$ and are pointwise functions of the state of the system. We distinguish two different values for each effective coefficient, the first corresponding to the regimes of ice uplift and free-surface flow ($D_{\text{eff,uf}}$ and $\mathbf{V}_{\text{eff,uf}}$), and the second corresponding to pressurized flow ($D_{\text{eff,p}}$ and $\mathbf{V}_{\text{eff,p}}$), yielding

$$D_{\text{eff,uf}} = \rho_w g\left(kh_w^{\alpha}+k_c S_w^{\alpha}\delta(\mathbf{x}_c)\right)|\nabla\phi|^{\beta-2}, \tag{19}$$

$$D_{\text{eff,p}} = e_v^{-1}\rho_w g\left(kh_w^{\alpha}+k_c S_w^{\alpha}\delta(\mathbf{x}_c)\right)|\nabla\phi|^{\beta-2}, \tag{20}$$

$$\mathbf{V}_{\text{eff,uf}} = k\alpha h_w^{\alpha-1}|\nabla\phi|^{\beta-2}\nabla\phi+h_w^{-1}Q\delta(\mathbf{x}_c)\hat{\mathbf{s}}, \tag{21}$$

$$\mathbf{V}_{\text{eff,p}} = h_w^{-1}\mathbf{q}+e_v^{-1}k_c\alpha R S_w^{\alpha-1}|\nabla\phi|^{\beta-2}\nabla\phi. \tag{22}$$

We then compute the time-step size Δt as

$$\Delta t = C\min\left(\frac{\min(\Delta x,\Delta y)^2}{4\max(D_{\text{eff,uf}},D_{\text{eff,p}})},\ \frac{\min(\Delta x,\Delta y)}{2\max\left(\|\mathbf{V}_{\text{eff,uf}}\|_\infty,\|\mathbf{V}_{\text{eff,p}}\|_\infty\right)}\right), \tag{23}$$

where C is a factor that we determine empirically. In the simulations, we find that $C=1/2$ is sufficient for stable time integration. The maximum is computed between all the local values at each grid cell, and $\|\cdot\|_\infty$ denotes the L_∞ norm.

An important consequence of the definitions in Eq. (19)–(22) is the key role of the parameter e_v on numerical performance. In pressurized flow, through both $D_{\text{eff, p}}$ and $\mathbf{V}_{\text{eff, p}}$, the order of magnitude of the time step bound largely relies on the order of magnitude of e_v. Namely, the runtimes for simulations with larger e_v (i.e., $e_v \geq 10^{-3}$) are significantly faster than those for simulations with smaller e_v (i.e., $e_v \leq 10^{-5}$).

https://doi.org/10.5194/egusphere-2026-4310
Preprint. Discussion started: 28 July 2026

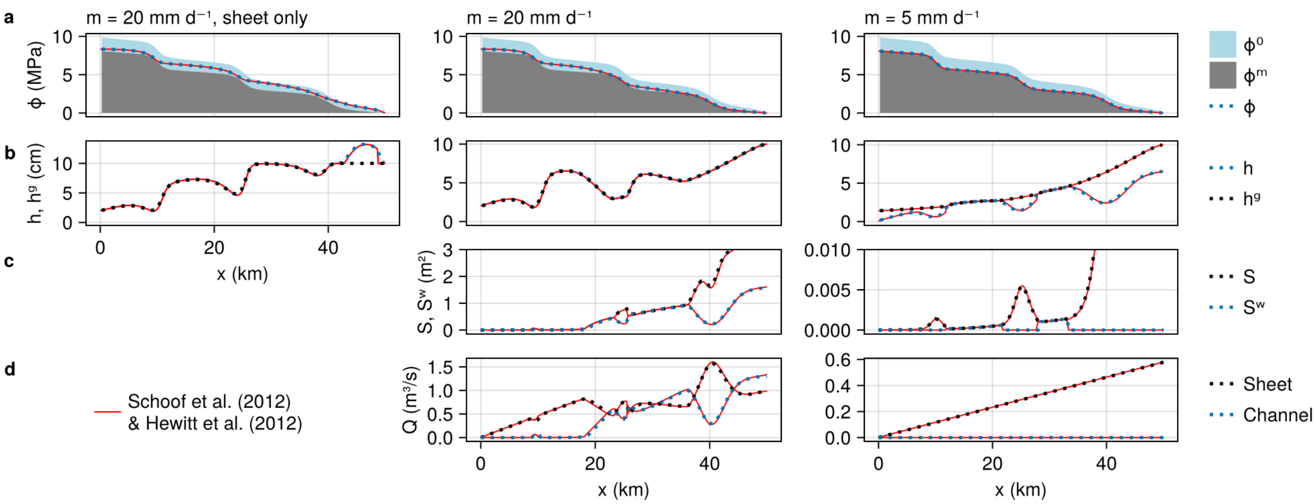

Figure 3. Three steady state drainage systems of a synthetic stepped glacier under uniform melt input m. Numerical results from GlaDS-2 are shown in dotted lines, and reference steady states from Schoof et al. (2012) and Hewitt et al. (2012) in solid red lines. The left column shows sheet-only model results, whereas the middle and right columns show coupled sheet and channel model results. Note the different y-axis scales across the different columns. (a) Hydraulic potential ϕ, bed elevation potential ϕ_m and overburden potential ϕ_0. (b) Water sheet height h and cavity height h_g. Regions with $h > h_g$ correspond to ice uplift, $h = h_g$ to pressurized flow, and $h < h_g$ to free-surface flow. (c) Channel cross-section S and water-filled cross-section S_w. Regions with $S_w = S$ correspond to fully-filled channels, and $S_w < S$ to partially-filled channels. (d) Channel discharge and width-integrated sheet discharge.

3 Model comparison

A core aim of our study is to extend the 1D numerical implementation of the model described in Schoof et al. (2012) and Hewitt et al. (2012) into 2D. Therefore, in this Section, we compare the results from our model to those of their implementation, hereafter referred to as the *1D implementation*, for a set of representative examples originally presented in the 2012 companion papers.

A key difference between the models is that our model incorporates englacial storage via the englacial void ratio e_v, whereas this component is absent from the 1D implementation. To allow for comparison between the two models, we set $e_v = 10^{-5}$ in our model. This value is chosen small enough to keep the englacial sheet height generally negligible, and large enough to not significantly impact model performance through its effect on reducing stable time-step size. Another difference is that, in the 1D implementation, the typical separation of channels is prescribed to 200 m (as the second dimension is not modeled), whereas in our 2D model the value of this separation is free to evolve and would appear as an output. However, as the edges of our numerical grid determine the possible locations of channels, we can impose the prescribed channel separation in our model through setting the grid spacing in the y direction to 200 m. The grid spacing in the x direction can be chosen freely for this

https://doi.org/10.5194/egusphere-2026-4310
Preprint. Discussion started: 28 July 2026

comparison, and we set its value to 500 m. Last, to compare our model to the 1D implementation, we display results along a 1D cross-section of our 2D domain.

The presented examples illustrate steady states of a synthetic stepped glacier under a uniformly distributed melt input. The examples are selected such that they span all three subglacial water pressure regimes in the sheet and all channel flow regimes, enabling to compare model behavior across all possible physical states.

In Fig. 3, at high melt input $m = 20$ mm d^{-1} and with sheet-only flow (left column), the steady state displays pressurized flow in all of the domain except near the terminus, where ice uplift occurs. With the same high melt input, the steady state with channels (middle column) no longer displays ice uplift, as channel opening allows the subglacial water pressure to decrease. In this case, sheet flow is pressurized throughout the domain. At lower melt input $m = 5$ mm d^{-1} (right column), the domain includes pressurized flow together with free-surface flow. The latter is present in regions where the drainage space is large enough to transport the water without needing to pressurize it, namely at the top of the domain, on the steeper slopes and at the terminus.

The steady state results also include all different regimes in channel flow. At the higher melt input (middle column), channels carry a significant portion of the subglacial discharge, and combine sections where they are fully water-filled on shallower slopes, and partially water-filled on steeper slopes and at the terminus. At lower melt input, channels remain small throughout the domain and the majority of subglacial flow is carried by the sheet. Channels are fully water-filled on shallower slopes, and are larger and empty on steeper slopes and at the terminus.

This comparison shows that the steady states reached by GlaDS-2 are mostly indistinguishable from those presented in Schoof et al. (2012) and Hewitt et al. (2012), throughout the different water pressure regimes in the sheet, the different regimes in channel flow, and the transitions between each of them. The same result extends to the other test cases featured in the companion papers. Although the two models differ in several details of their implementation, they reach equivalent steady-state solutions for all provided examples. We therefore conclude that our model can be used as an extension of the 1D implementation into 2D.

4 Simulation of a rapid supraglacial lake drainage

Rapid supraglacial lake drainages have been widely observed on the Greenland Ice Sheet (e.g., Das et al., 2008; Stevens et al., 2015; Chudley et al., 2019). In these events, millions of cubic meters of water are drained into the subglacial system within just a few hours. This sudden water input can temporarily induce ice flow acceleration as the water is drained downstream (Andrews et al., 2018; Mejia et al., 2021; Maier et al., 2023) through its effect on inducing ice uplift and decreasing effective pressure. Quantifying how subglacial water pressure and the surrounding drainage network evolve during these lake drainages is critical to understanding their impact on ice velocity and long-term ice sheet mass loss (Andrews et al., 2014; Maier et al., 2023).

We use GlaDS-2 to simulate a rapid supraglacial lake drainage both on synthetic (Sect. 4.1) and real topography (Sect. 4.2). Through these simulations, we demonstrate the model's capability to quantify transient subglacial water pressure dynamics

https://doi.org/10.5194/egusphere-2026-4310
Preprint. Discussion started: 28 July 2026

during and after lake drainage. Specifically, we capture the ice uplift driven by a propagating subglacial water blister and, by selecting a land-terminating glacier, we additionally simulate the transition to free-surface flow near the ice margins.

4.1 Synthetic topography

The synthetic topography is defined by a constant-sloped bed and a quadratically decreasing ice thickness (Fig. 4b). The spatial domain spans 50×15 km^2, where the last ~ 3 km along the x direction have zero ice thickness and thereby represent the proglacial region. We use a spatial resolution of 500×500 m^2, and impose an incoming subglacial sheet flux of 1 mm^2 s^{-1} on the upstream boundary (corresponding to 0.015 m^3 s^{-1} total inflow), zero flow on the lateral boundaries, and atmospheric pressure at the boundary in the proglacial zone. As initial conditions, we set the subglacial system at a steady state using a constant, uniformly distributed melt input of 1 mm d^{-1} (corresponding to ~8.7 m^3 s^{-1} total melt). The same melt input is maintained throughout the simulation.

To simulate the supraglacial lake drainage, we input the lake volume directly into the subglacial sheet into a single grid cell located at $(x,\ y) = (10,\ 7.5)$ km (Fig. 4a). We set the total lake volume to 44×10^6 m^3, and the total input time of the supraglacial lake to 1.4 h, matching the data used in the real topography runs (Sect. 4.2). For numerical stability, and because further details are not known, we input this volume as a parabolic pulse in time, from $t = 0$ to $t = 1.4$ h, with its peak at the half-time of this range. We track the response of the subglacial system to this lake drainage event by running the simulation for 300 h following the drainage onset.

Figure 4 illustrates the transient subglacial dynamics captured by the model during the simulated time period. The drained lake water volume induces localized ice uplift and propagates down-glacier as a traveling subglacial blister (Fig. 4a). The lake drainage has a clear impact on the subglacial water pressure throughout the simulation time (Fig. 4a–b). Shortly after the lake drainage, at $t = 2$ h, the increase in water pressure is confined to the area around the injection site, but subsequently expands to affect the entire modeled domain as the blister advances toward the terminus, most notably at $t = 90$ h.

As the subglacial blister travels downstream, its vertical profile alters significantly. In particular, the magnitude of ice uplift progressively decreases over time (Fig. 4c). This reduction in height is driven by the horizontal expansion of the blister, which allows water to leak laterally into the surrounding drainage system and accounts for the domain-wide pressure increase observed in the pressure fields.

At the glacier terminus, the model captures a dynamic transition in flow regimes (Fig. 4c–d). Prior to the subglacial blister reaching the terminus, the area shows free-surface flow at atmospheric pressure, both in the subglacial sheet and channels, up to ~ 6 km inward from the end of the domain (and, correspondingly, up to ~ 3 km inward from the glacier terminus). However, as the blister drains at the terminus, the terminal region temporarily switches to a state of high water pressure inducing ice uplift in the sheet, pressurizing the channels and increasing their size. This event at the terminus coincides with an increased water height in the proglacial zone, effectively capturing a rapid flooding behavior. Once the water volume in the subglacial blister has evacuated from the glacier, the terminal region returns to free-surface flow regime by 300 h.

The model also tracks the impact of the lake drainage on the subglacial channel system (Fig. 4d). Because this simulation uses a low melt input, no significant subglacial channel network is present prior to the drainage event. Consequently, while

https://doi.org/10.5194/egusphere-2026-4310
Preprint. Discussion started: 28 July 2026

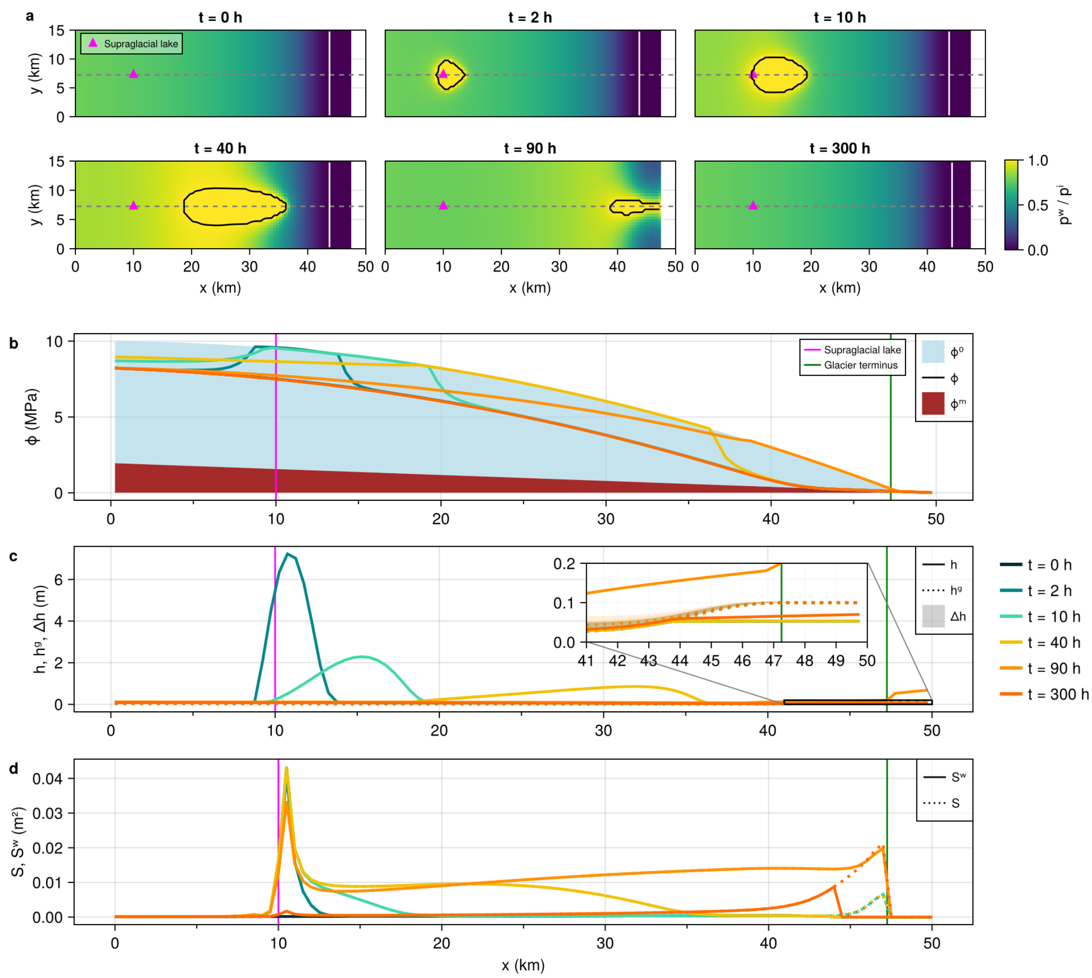

Figure 4. Time evolution of the subglacial system induced by the rapid drainage of a supraglacial lake on synthetic topography, through six representative time instances. (a) Snapshots of the flotation fraction p_w/p_i on the modeled domain. The area with $p_w/p_i = 1$ (outlined in black) contains ice uplift, while $p_w/p_i = 0$ (outlined in white) indicates free-surface flow. The gray dashed line shows the cross-section along which the 1D evolution of variables is plotted in (b). (b) Overlaid snapshots of the hydraulic potential ϕ. (c) Overlaid snapshots of the sheet thickness h, cavity height h_g, and englacial storage capacity thickness Δh. The subglacial sheet displays ice uplift where $h > h_g + \Delta h$, pressurized flow where $h_g \leq h < h_g + \Delta h$ and free-surface flow where $h < h_g$. (d) Overlaid snapshots of channel cross-section S, and water-filled cross-section S_w. Channels are fully filled where $S_w = S$, partially filled where $S_w < S$, and empty where $S_w = 0$. Regions with empty channels coincide with regions with free-surface flow in the sheet.

the sudden surge of lake water contributes to localized frictional channel melting, it is insufficient to, on its own, drive the development of a fully evolved channel network due to its short duration. The overall change in channel cross-sectional area remains small throughout the domain, leaving the subglacial system largely unchannelized both during and after the event.

https://doi.org/10.5194/egusphere-2026-4310
Preprint. Discussion started: 28 July 2026

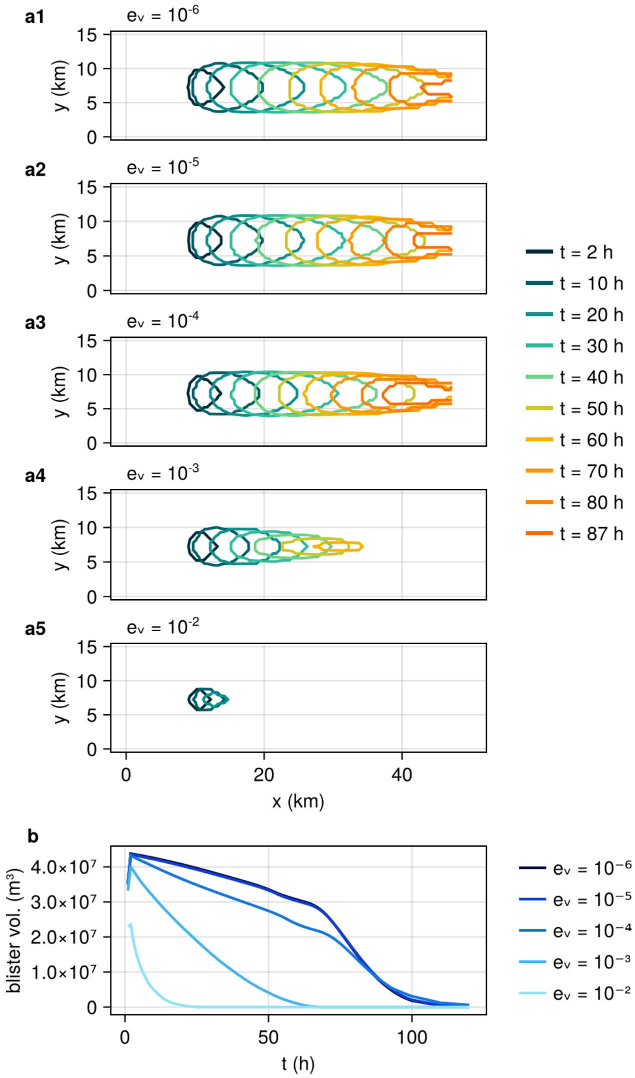

Figure 5. (a1)–(a5) Time evolution of the subglacial blister outlines on the synthetic topography for different values of the englacial void ratio e_v. (b) Comparison of subglacial blister volume over time for the different values of e_v. Note that the curves for $e_v = 10^{-6}$ and $e_v = 10^{-5}$ are overlapping.

The main persistent impact of the drainage is localized at the terminus, where a slightly enlarged channel remains visible at $t = 300$ h. In the terminal region, where ice thickness remains low, ice overburden pressure is insufficient to drive rapid viscous creep closure, allowing the enlarged channel to persist after the lake drainage event.

https://doi.org/10.5194/egusphere-2026-4310
Preprint. Discussion started: 28 July 2026

4.1.1 Dependency on e_v parameter

The englacial void ratio e_v plays a key role in our model in two distinct ways. First, it acts as the regularization parameter in the equation relating water pressure to subglacial sheet height (Eq. (4)). Second, it carries physical meaning by modulating the volume of water that is stored englacially. While this physical behavior does not alter steady-state configurations, it strongly influences transient subglacial dynamics (Werder et al., 2013).

To illustrate the dependency of our results on this parameter, we reproduce the synthetic topography simulation (Fig. 4a) for values of e_v ranging from 10^{-6} to 10^{-2}. In Fig. 5, we show the different time evolution of the resulting subglacial blister resulting from each value of e_v.

The modeled outlines of the subglacial blister (Fig. 5a) show that its location and spatial extent are nearly identical for $e_v = 10^{-6}$ and $e_v = 10^{-5}$. At these lower values, the englacial storage capacity is virtually zero, meaning the parameter affects only computational efficiency through its impact on the time-step size. This effect is further confirmed by the evolution of the subglacial blister volume (Fig. 5b), which we calculate as the integral of $h_w - h_g$ over its area. The volume curves are indistinguishable between $e_v = 10^{-6}$ and $e_v = 10^{-5}$, where e_v acts solely as a regularization parameter and does not represent a physically impactful storage term in the system.

Increasing the englacial void ratio to $e_v = 10^{-4}$ produces minor variations in the response of the subglacial system to the supraglacial lake drainage. The blister propagates down-glacier slightly more slowly, covers a marginally smaller lateral area (Fig. 5a), and maintains a slightly lower volume and thus less ice uplift throughout the simulation (Fig. 5b). This variation is driven by a fraction of the blister volume being incorporated into the available englacial storage. A larger englacial void ratio of $e_v = 10^{-3}$ results in a marked increase in this physical behavior of the system: a much higher amount of water can be held in englacial storage, allowing the blister to be accommodated englacially before the blister can reach the terminus. As a result, the blister travels only about half the distance and persists for about half the time compared to the $e_v = 10^{-4}$ case. This attenuation is even more pronounced at $e_v = 10^{-2}$, where the blister remains highly localized, persists for only approximately 20 h, and is rapidly absorbed by the surrounding englacial storage capacity.

4.1.2 Dependency on channelization

The response of the subglacial system to rapid supraglacial lake drainage depends fundamentally on its preexisting state. A channelized system—typical of high-melt summer conditions—drives a markedly different evolution of induced ice uplift than a distributed system characterizing low-melt winter conditions. Due to their greater localized flow efficiency, channels accelerate both the propagation and the drainage of the subglacial blister.

We illustrate the effect of channelization on our results by reproducing the synthetic topography simulation (Fig. 4a) using two different distributed melt inputs: a high-melt scenario of $m = 20$ mm d^{-1} and the original low-melt scenario of $m = 1$ mm d^{-1}. Under the high-melt conditions, the steady-state system is channelized across a large portion of the domain (Fig. 6a). For this comparison, we use a smaller lake volume of 20×10^6 m^3 to prevent the high-melt drainage from overflowing the domain boundary.

https://doi.org/10.5194/egusphere-2026-4310
Preprint. Discussion started: 28 July 2026

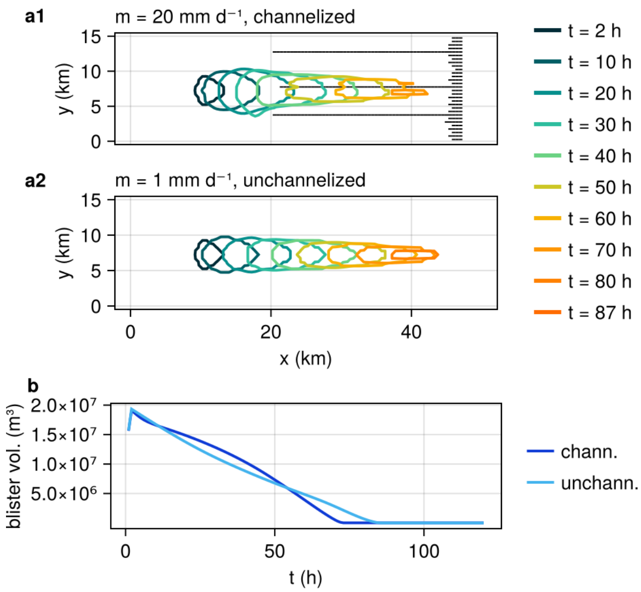

Figure 6. (a1)–(a2) Time evolution of the subglacial blister outlines on the synthetic topography for different values of melt input and corresponding channelization. The black lines in (a1) indicate the locations of subglacial channels carrying discharge $Q > 1\ \mathrm{m^3\ s^{-1}}$. (b) Comparison of subglacial blister volume over time for the two different melt forcings and corresponding channelization.

The modeled subglacial blister outlines (Fig. 6a) show distinct differences between the two scenarios. At high melt input, the subglacial blister initially ($t < 20$ h) extends over a larger horizontal area and travels more slowly than with a low melt input, characteristic of a distributed system that is previously heavily pressurized by melt and has reduced available englacial storage capacity. As the blister reaches the developed channel network ($t \geq 20$ h, $x > 20$ km), its propagation accelerates as a portion of the blister volume is accommodated into efficient channel flow. The acceleration is strongest in sections of the blister aligned with channel pathways, which effectively reshapes its geometry. Consequently, by $t = 80$ h, the intersecting channel has split the original shape into two distinct, smaller blisters.

The time evolution of the blister volume (Fig. 6b) further reflects how channelization impacts drainage speed. As the blister increasingly extends into the channelized domain, its total volume decreases at an accelerating rate compared to the low-melt, unchannelized case. Ultimately, the blister is completely drained ~ 10 h earlier under channelized conditions, even considering that this system must evacuate a significantly larger volume of background melt.

4.2 Real topography: North Lake in Greenland

To show the applicability of the GlaDS-2 to a real-world setting, we run the model for a drainage of North Lake (68.72°N, −49.50°W) in Greenland as described in Das et al. (2008). We use the bed elevation and ice thickness data from BedMachine v6 (Morlighem et al., 2020, 2025). The spatial domain in our simulation is ∼7500 km^2, and covers the region between

https://doi.org/10.5194/egusphere-2026-4310
Preprint. Discussion started: 28 July 2026

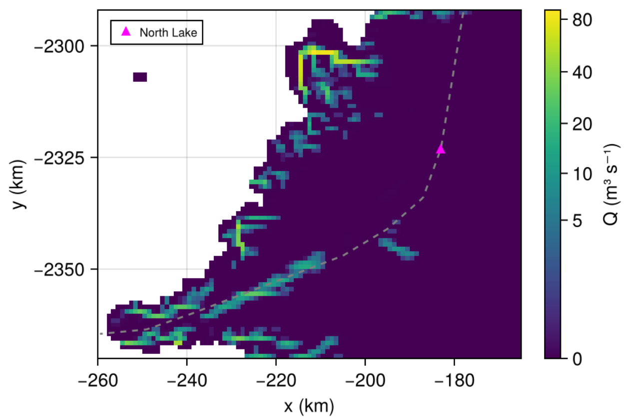

Figure 7. Map view of the model domain for the North Lake simulation, in western Greenland. Channel flow Q averaged per grid cell on the modeled domain, after 400 days of evolution of the subglacial system under the temperature index model detailed in Eq. (24)–(25). This state of the subglacial system is set as the initial condition in the supraglacial lake drainage simulation on real topography. The gray dashed curve shows the cross-section along which the subglacial system is plotted in Fig. 8. Data is shown only for the ice-covered domain. Spatial coordinates are in EPSG:3413 coordinate system, the underlying topographical data is from BedMachine v6 (Morlighem et al., 2025).

approximately 68.25°N−69.02°N latitude and 49.05°W−51.47°W longitude (Fig. 7). We use a spatial resolution of 1000×1000 m^2, and impose zero-flow conditions on all four domain boundaries. While this is a simplification that reduces the validity of results near the boundaries and at the proglacial zone, it simplifies the numerical implementation and should not significantly affect the area influenced by the supraglacial lake drainage. As initial condition for the lake drainage, we let the subglacial system evolve to near a steady state over 400 days, after which the evolution of the system becomes negligible, except at the proglacial zone as a consequence of the imposed no-flow conditions. As forcing we use melt typical for early-summer temperatures, using a temperature index model for calculating the melt throughout the domain. With this model, the melt input m at each point (x, y) is defined as

$$m(x,y) = c_1 \max\left(0, T(x,y)\right), \tag{24}$$

where we set the melt factor to $c_1 = 2 \times 10^{-8}$ m s^{-1} K^{-1} (producing early-summer melt values consistent with Stevens et al. (2018) in the same region), and

$$T(x,y) = T_0 + c_2\left(E(x,y) - E_0\right), \tag{25}$$

where $T_0 = 11$°C is the average early-summer temperature at the nearest weather station in Kangerlussuaq, the lapse rate is $c_2 = -0.006$ K m^{-1}, $E(x,y)$ is the surface elevation, and $E_0 = 50$ m is the elevation of the weather station. Running the model on the domain with this melt input over 400 days, we find that a significant portion of the subglacial system becomes channelized (Fig. 7). The same temperature, and therefore melt input distribution, is maintained throughout the supraglacial lake drainage simulation.

https://doi.org/10.5194/egusphere-2026-4310
Preprint. Discussion started: 28 July 2026

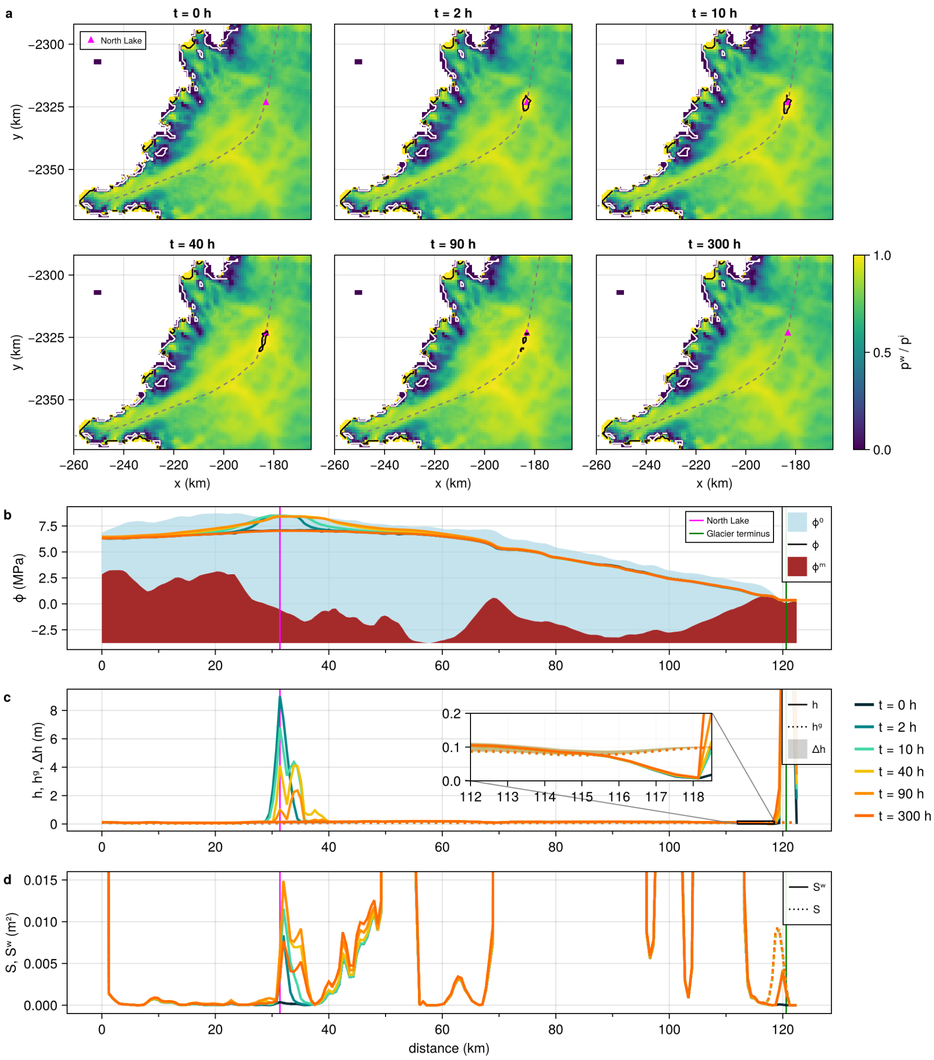

Figure 8. Time evolution of the subglacial system induced by the rapid drainage of North Lake, through six representative time instances. (a) Snapshots of the flotation fraction p_w/p_i on the modeled domain. The area with $p_w/p_i = 1$ (outlined in black) contains ice uplift, while $p_w/p_i = 0$, (outlined in white) indicates free-surface flow. The gray dashed curve shows the cross-section along which the 1D evolution of variables is plotted in (b). (b) Overlaid snapshots of hydraulic potential ϕ. (c) Overlaid snapshots of sheet thickness h, cavity height h_g, and englacial storage capacity thickness Δh. The subglacial sheet displays ice uplift where $h > h_g + \Delta h$, pressurized flow where $h_g \leq h < h_g + \Delta h$ and free-surface flow where $h < h_g$. (c) Overlaid snapshots of channel cross-section S, and water-filled cross-section S_w. Channels are fully filled where $S_w = S$, partially filled where $S_w < S$, and empty where $S_w = 0$. Regions with empty channels coincide with regions with free-surface flow in the sheet. In b–d, the horizontal axis marks the distance traveled along the curve drawn in (a), in the direction from northeast to southwest. The underlying topographical data for panels (a) & (b) is from BedMachine v6 (Morlighem et al., 2025).

https://doi.org/10.5194/egusphere-2026-4310
Preprint. Discussion started: 28 July 2026

To simulate the supraglacial lake drainage, we follow the same approach as described for the synthetic topography: we input the lake volume directly into the subglacial sheet, into a single grid cell at the location of North Lake (Fig. 8a). We set the total lake volume to 44×10^6 m^3, and the total input time of the supraglacial lake to 1.4 h, as detailed in the first documented drainage of North Lake in Das et al. (2008). Again for numerical stability and because further details remain unknown, we input this volume as a parabolic pulse in time, from $t = 0$ to $t = 1.4$ h, with its peak at the half-time of this range. We track the response of the subglacial system to this lake drainage event by running the simulation for the 300 h following the drainage onset.

Figure 8 shows the transient subglacial dynamics captured by the model during the simulated time period in response to the drainage of North Lake. The drained lake water volume induces localized ice uplift, which propagates a few kilometers downstream as a traveling subglacial blister (Fig. 8a). The lake drainage has a clear impact on the subglacial water pressure throughout the simulation time (Fig. 8a–b). Shortly after the lake drainage, at $t = 2$ h, the increase in water pressure is restricted to the area around the injection site, but in time expands to affect an area spanning tens of kilometers in each horizontal direction, as the blister advances along its flow path and leaks into the surrounding subglacial drainage system.

The vertical profile of the subglacial blister evolves as it travels downstream. Its height progressively decreases over time and reacts to the geometry of the local topography (Fig. 8c). As the blister thickness decreases, it expands horizontally and simultaneously leaks into the surrounding drainage system, resulting in the increased values observed in the pressure field. Notably, ice uplift is also reduced as the blister reaches the beginning of the channel network (Fig. 8c–d).

The model captures the free-surface flow regime occurring near the ice margins across a large portion of the glacier outline (Fig. 8a), and is also reflected in both the sheet and channels near the terminus (Fig. 8c–d). Unlike in the synthetic topography simulation, where the subglacial blister drains at the terminus, here the blister volume is accommodated locally within the inland subglacial system. Therefore, the blister drainage neither directly affects the flow regime closer to the margin, nor increases the channel size at the terminus. However, the free-surface flow regime at the terminus does evolve throughout the simulation, which can be attributed to the no-flow boundary conditions enforced in this simulation. Where a constant sea-level water height h would be expected in this proglacial region, the restriction of outward flux effectively models a proglacial lake that continuously fills with glacier water discharge. This progressive filling mechanism is captured by the rising water levels at the terminus in both the sheet and channels over time.

This simulation uses a relatively high melt input, under which a developed channel network is present prior to the drainage event (Fig. 7). Therefore, the results also display the interaction of the lake drainage with the preexisting subglacial channel system (Fig. 8d). At the lake location, which is initially unchannelized, the sudden water injection contributes to localized melting of channels that gradually close due to ice creep once ice uplift has subsided, mirroring what is observed in the synthetic results on an unchannelized domain. A transition in behavior occurs upon reaching preexisting channels at ~ 40 km along the plotted curve. As the blister intersects the channels, the sudden influx of water drives a minor increase in their cross-section, which persists throughout the simulation, outlasting the subsidence of ice uplift in the sheet. While the lake drainage has a low overall impact on the channel network, conversely, these results are consistent with the marked impact of a developed

https://doi.org/10.5194/egusphere-2026-4310
Preprint. Discussion started: 28 July 2026

early-summer channel network on reducing ice uplift by enabling the efficient subglacial system to rapidly accommodate the drained water volume.

5 Discussion

5.1 Modeling approach and contributions

Subglacial water flow frequently spans regimes that differ from the assumptions of existing two-dimensional drainage models—namely that neither ice uplift nor free-surface flow occurs. In reality, excess water volume is accommodated through ice uplift once water pressure exceeds ice overburden pressure. At the other extreme, instead of dropping to unphysical negative values, subglacial pressure remains at atmospheric levels as channels and cavities transition to free-surface flow. Until now, incorporating these physical behaviors has been computationally tractable only in one dimension (Schoof et al., 2012; Hewitt et al., 2012). The main contribution of this work is the GlaDS-2 model, which addresses this gap by incorporating all three pressure regimes (pressurized flow, ice uplift, and free-surface flow) into a two-dimensional framework, while handling the transitions between them without the need for solving the computationally demanding free-boundary problem as was done in the previous one-dimensional implementation.

To date, modeling subglacial drainage in the presence of ice uplift and free-surface flow has relied on formulating a free-boundary problem using variational inequalities (Schoof et al., 2012; Hewitt et al., 2012). This approach then necessitated to solve different equations in each of the regions. In our model, we instead solve the same set of equations in all regions and use a closure relation (Eq. (4)) to determine the water pressure as a function of the water sheet thickness. This constitutes a front-capturing approach, and requires a conservative discretization, which we implement in our method. As an advantage of this approach, mass conservation is built into the model by construction.

Fundamentally, this framework is analogous to the enthalpy method used in ice temperature modeling (e.g., Aschwanden et al., 2012). Rather than explicitly tracking the cold-temperate transition boundary, the enthalpy method solves a single conservation equation for energy across the entire domain, paired with a thermodynamic equation of state relating energy and temperature. In our formulation, the closure relation (Eq. (4)) serves as the direct equivalent to this equation of state, enabling a similarly unified approach. Another method to which our framework is analogous to is the Preismann slot method in hydraulics (Preissmann and Cunge, 1961; Cunge and Wegner, 1964). This method was established to simulate both free-surface and pressurized flow in a tunnel using the one-dimensional shallow water equation (more recently, a two dimensional extension was established (Maranzoni et al., 2015)). It adds a thin slot above the tunnel to change the pressurized flow into free-surface flow, albeit with a very rapidly-varying water level. This slot is analogous to our englacial storage, which makes water volume related algebraically to water pressure via the closure relation.

GlaDS-2 improves on the original GlaDS (Werder et al., 2013) in a number of ways. Unlike GlaDS, it is capable of handling strongly variable water inputs due to the inclusion of ice uplift. This physical omission in the original model manifested as frequent, widespread overpressure (p_w exceeding overburden pressure) during seasonal simulations of alpine glaciers (Werder et al., 2013). Another example of this behavior would be the supraglacial lake drainage presented here, where the original

https://doi.org/10.5194/egusphere-2026-4310
Preprint. Discussion started: 28 July 2026

GlaDS would simulate extreme overpressures coupled with a very slow deflation of the subglacial blister. While the drainage model of Hewitt (2013), which is similar to GlaDS, was later modified to include elastic sheet uplift (Banwell et al., 2016; Stevens et al., 2022), this addition only partially mitigates overpressure rather than preventing it entirely. Including free-surface flow also resolves a number of issues in the original model. It improves boundary condition handling: First, no-flow conditions can now be prescribed on mountain-glacier flanks and ice-sheet margins without inducing spurious negative pressures. Second, users no longer need to manually pre-determine and place outflow Dirichlet points to prevent the numerical instabilities that occur when these outlets inadvertently become water inflow points. Moreover, the free-surface flow regime allows GlaDS-2 to also seamlessly simulate proglacial water flow. Remarkably, even though GlaDS-2 extends the original model with new physics, it retains the exact same set of physical parameters.

By successfully reproducing the results of the only previous model that incorporated all three subglacial water pressure regimes (Schoof et al., 2012; Hewitt et al., 2012), we verify that our mathematical formulation (which is equivalent to theirs as $e_v \to 0$) and its numerical implementation are sound. Consistent with these previous studies, ice uplift occurs in steady-state configurations only when no channels are modeled. When channels are present, ice uplift arises only in transient conditions or where there is a depression in the hydraulic potential (e.g., Clarke, 2005). Free-surface flow, on the other hand, occurs on steep sections and is more prevalent at lower discharge. This is supported by early theoretical work (Hooke, 1984), tracer experiments (e.g. Seaberg et al., 1988), and recent seismic noise observations (Gimbert et al., 2016). Moreover, free-surface flow can be present in partially-filled channels while the flow in adjacent subglacial cavities remains pressurized.

5.2 Application to rapid supraglacial lake drainages

The rapid drainage of a supraglacial lake on a land-terminating glacier, represented by our synthetic topography simulations (Sect. 4.1) and by the Greenland Ice Sheet sector in our real topography simulations (Sect. 4.2), is an ideal test case for these regimes. This scenario exhibits transient ice uplift induced by a subglacial blister forming around the lake injection site, free-surface flow at the ice margins and in the proglacial zone, and rapid fluctuations in subglacial water pressure as the lake drains in a matter of hours. While this setup has been simulated by previous models (Tsai and Rice, 2010; Dow et al., 2015; Lai et al., 2021; Zhang et al., 2025), our model is the first general-purpose subglacial model to simulate such behavior in 2D, without requiring the addition of extra model components such as separate blister or hydrofracture models.

We use our experiments on subglacial blister evolution (Sect. 4.1) to demonstrate the dual role that the englacial void ratio e_v plays in our model: while it serves as a numerical regularization parameter for $e_v \leq 10^{-5}$, it acts as a physical parameter driving a distinct evolution of subglacial water pressure regimes for $e_v \geq 10^{-4}$. The supraglacial lake drainage simulations spanning these different englacial storage cases are consistent with the interpretation of a large englacial void ratio acting as a damping term for subglacial water pressure fluctuations (Werder et al., 2013). Specifically, our model results demonstrate that this damping directly impacts the persistence of ice uplift induced by the drainage, by limiting both its spatial and temporal extent. A similar role of englacial storage in subglacial blister dissipation was identified by Stevens et al. (2022), and this influence was found to be smaller than that of sheet conductivity.

https://doi.org/10.5194/egusphere-2026-4310
Preprint. Discussion started: 28 July 2026

The interaction between a rapid supraglacial lake drainage and the subglacial channel network is modeled in our experiments on synthetic (Sect. 4.1) and real (Sect. 4.2) topographies. Our results show how a developed channel network affects the response of the subglacial system to the large water volume input, accelerating the propagation of the subglacial water blister and, consequently, the subsidence of the induced ice uplift. Moreover, the model results indicate that the short duration of the lake drainage is insufficient to force the development of an efficient subglacial channel network on its own (contrary to what was previously postulated by e.g., Sole et al. (2011) and Cowton et al. (2013)). This absence of significant channelization induced by the lake drainage is consistent with both the 1D elastic modeling implemented by Dow et al. (2015) and the direct observations of Mejia et al. (2021), which demonstrate the dominant role of the preexisting subglacial system in the pressure reduction following the drainage. Moreover, our simulated blister evolution aligns closely with the 2D blister model by Zhang et al. (2025), where the subglacial blister decays rapidly under summertime conditions and is split into two parts as water is routed into an intersecting channel.

Overall, the rapid lake drainage simulation of North Lake in Greenland (Sect. 4.2) demonstrates the model's capabilities on real topography. A precise reconstruction of this specific event is beyond the scope of this study and would require site-specific parameter calibration (in particular, the sheet conductivity has been found to be a critical parameter governing the blister size and dissipation (Lai et al., 2021; Stevens et al., 2022)), concurrent topographic and drainage data, and boundary conditions derived from a catchment runoff study. Nonetheless, our model predicts subglacial blister dimensions and ice uplift duration at the ice-bed interface (up to ~ 8 m height, ~ 5 to 10 km width, and ~ 4 days, respectively) that agree well with measured surface values for North Lake drainages (~ 0.7 to 2 m height, ~ 5 km width, and ~ 1 to 10 days reported in Das et al. (2008); Stevens et al. (2015, 2024)). The remaining discrepancy is consistent with our subglacial model not being coupled to an ice-flow model. This coupling would impact the modeled surface blister dimensions and duration by accounting for stress redistribution within the overlying ice and elastic deformation during the early stages of blister evolution.

Our simulations additionally showcase the model's ability to represent transient proglacial environments. In the synthetic case (Sect. 4.1), the model captures a transient proglacial flooding event, onset by the drainage of the subglacial blister at the terminus. On real topography (Sect. 4.2), imposing a no-flow boundary condition effectively models a proglacial lake filling with discharge over time. Integrating these proglacial flow dynamics into subglacial modeling follows from the inclusion of free-surface flow, and offers a distinct advantage for understanding the downstream impacts of subglacial drainage processes, such as flood wave propagation or sediment transport.

5.3 Model limitations and future directions

A current limitation of GlaDS-2 is its reduced numerical performance due to the constraints on the time step size (Sect. 2.5). For the simulations presented in this work, time-step sizes range from tenths of a second to tens of seconds, with runtimes spanning from a few minutes to several days on a single CPU. A future version of GlaDS-2 should incorporate implicit time integration, which would enable significantly higher performance by allowing time-step sizes on the order of hours to days, enabling simulations at finer resolutions and across broader parameter ranges. Furthermore, because all our model components are paralellizable, we envision improving model performance by porting the next version of GlaDS-2 to GPUs.

https://doi.org/10.5194/egusphere-2026-4310
Preprint. Discussion started: 28 July 2026

A further limitation of GlaDS-2 is that its structured rectangular grid constrains the geometry of the emergent channel network, as channel formation is only allowed along grid edges. This introduces a directional bias, which is particularly pronounced when a channel should naturally follow a diagonal path relative to the grid. This grid limitation is common to other structured-grid models (e.g., Schoof, 2010), and its impact can be mitigated in a future model version by incorporating channels located at diagonal grid edges (e.g., Hewitt, 2013).

As with other subglacial drainage models, direct validation of GlaDS-2 is constrained by the inherent difficulties of accessing and measuring the subglacial environment *in situ*. Consequently, model validation must rely on contextualizing borehole measurements in 2D, and on indirect proxies. Because our model explicitly simulates physical ice uplift and transitions to free-surface flow, its transient outputs can be indirectly evaluated against surface displacement measurements, as we performed for our subglacial blister comparison, as well as against ice dynamics changes (e.g., Riesen et al., 2010), or seismic signatures of turbulent channelized flow (e.g., Gimbert et al., 2016). The model's ability to simulate proglacial water flow dynamics opens new avenues for catchment-scale validation by comparing simulated outflow magnitude and locations, and transit velocities against terminal discharge measurements and dye-tracer travel times. Thus, at least the overall efficiency and routing behavior of the modeled drainage network could be evaluated without requiring direct access to the glacier bed. However, the main avenue to make use of the available direct and indirect observations would be to integrate parameter inversion capabilities into our model. Tracer transit times and borehole observations have been shown to partially constrain GlaDS parameters (Irarrazaval et al., 2019, 2021). However, ice dynamics observations can also be leveraged if a coupled subglacial drainage and ice-flow model is inverted. Brinkerhoff et al. (2021) used such a coupled model inversion for a sector of the West Greenland ice sheet to provide the best estimates to date of key GlaDS parameters.

Further work includes coupling GlaDS-2 to an ice-flow model. Without this coupling, we assume hydrostatic ice-overburden pressure, a static ice thickness, and a prescribed sliding velocity that contributes to cavity opening. As a consequence of the hydrostatic assumption, ice uplift occurs instantly as water pressure reaches ice overburden pressure. In reality, ice uplift would require pressures exceeding overburden pressure to initiate ice deformation. This overpressure of the subglacial water would result in a locally non-hydrostatic stress distribution within the ice, resulting in ice deformation, lateral stress coupling and changes in ice thickness. On short time scales, such as for supraglacial lake drainages in Greenland, the deformation would occur elastically, whereas on longer time scales, such as for slowly draining and filling subglacial lakes in Antarctica, the deformation would be viscous. Adequately representing these processes would require coupling a fully three-dimensional ice-flow model with visco-elastic ice rheology. Applying the coupled model at continental scale would likely require parameterizing uplift-related, non-hydrostatic processes so that they could be represented within simpler, more computationally efficient depth-integrated ice-flow models, such as DIVA (Goldberg, 2011).

6 Conclusions

In this study, we have presented GlaDS-2, a new subglacial drainage model that builds upon the original GlaDS (Werder et al., 2013) and that uses a novel, unified formulation to incorporate the subglacial regimes of ice uplift and free-surface flow as

https://doi.org/10.5194/egusphere-2026-4310
Preprint. Discussion started: 28 July 2026

described in Schoof et al. (2012) and Hewitt et al. (2012). We improve on these previous studies by extending the numerical model from one to two spatial dimensions. Adding the free-surface flow regime additionally improves the tractability of setting boundary conditions, and integrates proglacial water flow modeling. Our implementation ensures mass conservation, allowing implicit capturing of the boundaries separating different flow regimes.

We have demonstrated the model's capabilities by simulating a rapid supraglacial lake drainage event on both synthetic topography and real topography from North Lake in Greenland (Das et al., 2008). Our model simulates the formation of a traveling subglacial blister inducing ice uplift, and captures regions of free-surface flow at the ice margins. Notably, the predicted spatial extent and duration of ice uplift on real topography agree in order of magnitude with on-site observations (Das et al., 2008; Stevens et al., 2015, 2024).

Through a parameter sensitivity study, we show that englacial storage and preexisting channelization in the subglacial system strongly influence the spatial and temporal extent of ice uplift induced by such rapid drainage events. Our findings align with previous work indicating that while dissipation of the subglacial blister is dominantly mediated by the distributed subglacial system, this behavior shifts when a pre-established channel network is present (Dow et al., 2015; Mejia et al., 2021; Zhang et al., 2025).

These advancements in GlaDS-2 lay the foundation for improving future coupling of subglacial drainage to ice-flow models, by providing physically consistent subglacial water pressures to constrain and employ in basal sliding laws. Integrating this subglacial framework with an ice-flow solver will enable a more realistic representation of how transient ice uplift and free-surface flow modulate glacier velocities and, ultimately, govern the long-term evolution of glaciers and ice sheets.

Code and data availability. The exact version of the code to reproduce results and figures of this paper is archived on Zenodo (https://doi.org/10.5281/zenodo.21470407, note this is the link for the reviewer-restricted code. Publicly available code will be released on zenodo on publication.). Present and future releases of the code can be also accessed on GitHub (https://github.com/swellsc/GlaDS-2, released on publication). Running the simulation of a rapid supraglacial lake drainage on the real topography requires access to BedMachne v6 (Morlighem et al., 2025), which is available for free under the NASA National Snow and Ice Data Center (NSIDC) Use and Copyright policy (https://nsidc.org/about/data-use-and-copyright).

Author contributions. SW, MW, and IU designed the study and developed, together with IH, the mathematical and numerical formulations; IU deviced the closure-relation approach to unify the three pressure regimes; SW coded the numerical implementation and performed all simulations; SW, MW and DF analyzed the output; SW, IH, and MW prepared Figure 1; SW prepared the manuscript and figures with contributions from all co-authors.

Competing interests. At least one of the (co-)authors is a member of the editorial board of The Cryosphere. The authors have no other competing interests to declare.

https://doi.org/10.5194/egusphere-2026-4310
Preprint. Discussion started: 28 July 2026

Acknowledgements. This research was supported by SNF project no. 10002436 "Glacier Lakes in Antarctica: Drainage, Dynamics, Evolution and Refilling (GLADDER)". Large language models (Claude Sonnet 4.6, Gemini 3.5) were used to edit sentences and to help create Fig. 1b.

https://doi.org/10.5194/egusphere-2026-4310
Preprint. Discussion started: 28 July 2026

References

Andrews, L. C., Catania, G. A., Hoffman, M. J., Gulley, J. D., Lüthi, M. P., Ryser, C., Hawley, R. L., and Neumann, T. A.: Direct Observations of Evolving Subglacial Drainage beneath the Greenland Ice Sheet, Nature, 514, 80–83, https://doi.org/10.1038/nature13796, 2014.

Andrews, L. C., Hoffman, M. J., Neumann, T. A., Catania, G. A., Lüthi, M. P., Hawley, R. L., Schild, K. M., Ryser, C., and Morriss, B. F.: Seasonal Evolution of the Subglacial Hydrologic System Modified by Supraglacial Lake Drainage in Western Greenland, Journal of Geophysical Research: Earth Surface, 123, 1479–1496, https://doi.org/10.1029/2017JF004585, 2018.

Aschwanden, A., Bueler, E., Khroulev, C., and Blatter, H.: An Enthalpy Formulation for Glaciers and Ice Sheets, Journal of Glaciology, 58, 441–457, https://doi.org/10.3189/2012JoG11J088, 2012.

Banwell, A., Hewitt, I., Willis, I., and Arnold, N.: Moulin Density Controls Drainage Development beneath the Greenland Ice Sheet, Journal of Geophysical Research: Earth Surface, 121, 2248–2269, https://doi.org/10.1002/2015JF003801, 2016.

Beyer, S., Kleiner, T., Aizinger, V., Rückamp, M., and Humbert, A.: A Confined–Unconfined Aquifer Model for Subglacial Hydrology and Its Application to the Northeast Greenland Ice Stream, The Cryosphere, 12, 3931–3947, https://doi.org/10.5194/tc-12-3931-2018, 2018.

Brinkerhoff, D., Aschwanden, A., and Fahnestock, M.: Constraining Subglacial Processes from Surface Velocity Observations Using Surrogate-Based Bayesian Inference, Journal of Glaciology, 67, 385–403, https://doi.org/10.1017/jog.2020.112, 2021.

Bueler, E. and van Pelt, W.: Mass-Conserving Subglacial Hydrology in the Parallel Ice Sheet Model Version 0.6, Geoscientific Model Development, 8, 1613–1635, https://doi.org/10.5194/gmd-8-1613-2015, 2015.

Chudley, T. R., Christoffersen, P., Doyle, S. H., Bougamont, M., Schoonman, C. M., Hubbard, B., and James, M. R.: Supraglacial Lake Drainage at a Fast-Flowing Greenlandic Outlet Glacier, Proceedings of the National Academy of Sciences, 116, 25 468–25 477, https://doi.org/10.1073/pnas.1913685116, 2019.

Clarke, G. C. K.: Subglacial Processes, Annual Review of Earth and Planetary Sciences, 33, 247–276, https://doi.org/10.1146/annurev.earth.33.092203.122621, 2005.

Cook, S. J., Christoffersen, P., and Todd, J.: A Fully-Coupled 3D Model of a Large Greenlandic Outlet Glacier with Evolving Subglacial Hydrology, Frontal Plume Melting and Calving, Journal of Glaciology, 68, 486–502, https://doi.org/10.1017/jog.2021.109, 2022.

Cowton, T., Nienow, P., Sole, A., Wadham, J., Lis, G., Bartholomew, I., Mair, D., and Chandler, D.: Evolution of Drainage System Morphology at a Land-terminating Greenlandic Outlet Glacier, Journal of Geophysical Research: Earth Surface, 118, 29–41, https://doi.org/10.1029/2012JF002540, 2013.

Cunge, J. A. and Wegner, M.: Intégration Numérique Des Équations d'écoulement de Barré de Saint-Venant Par Un Schéma Implicite de Différences Finies, La Houille Blanche, 50, 33–39, https://doi.org/10.1051/lhb/1964002, 1964.

Das, S. B., Joughin, I., Behn, M. D., Howat, I. M., King, M. A., Lizarralde, D., and Bhatia, M. P.: Fracture Propagation to the Base of the Greenland Ice Sheet During Supraglacial Lake Drainage, Science, 320, 778–781, https://doi.org/10.1126/science.1153360, 2008.

de Fleurian, B., Gagliardini, O., Zwinger, T., Durand, G., Le Meur, E., Mair, D., and Råback, P.: A Double Continuum Hydrological Model for Glacier Applications, The Cryosphere, 8, 137–153, https://doi.org/10.5194/tc-8-137-2014, 2014.

Dow, C. F., Kulessa, B., Rutt, I. C., Tsai, V. C., Pimentel, S., Doyle, S. H., Van As, D., Lindbäck, K., Pettersson, R., Jones, G. A., and Hubbard, A.: Modeling of Subglacial Hydrological Development Following Rapid Supraglacial Lake Drainage: MODELING LAKE DRAINAGE HYDROLOGY, Journal of Geophysical Research: Earth Surface, 120, 1127–1147, https://doi.org/10.1002/2014JF003333, 2015.

Dow, C. F., Werder, M. A., Nowicki, S., and Walker, R. T.: Modeling Antarctic Subglacial Lake Filling and Drainage Cycles, The Cryosphere, 10, 1381–1393, https://doi.org/10.5194/tc-10-1381-2016, 2016.

Downs, J., Johnson, J., Harper, J., Meierbachtol, T., and Werder, M.: Dynamic Hydraulic Conductivity Reconciles Mismatch between Modeled and Observed Winter Subglacial Water Pressure, Journal of Geophysical Research, 123, https://doi.org/10.1002/2017JF004522, 2018.

Ehrenfeucht, S., Morlighem, M., Rignot, E., Dow, C. F., and Mouginot, J.: Seasonal Acceleration of Petermann Glacier, Greenland, From Changes in Subglacial Hydrology, Geophysical Research Letters, 50, e2022GL098 009, https://doi.org/10.1029/2022GL098009, 2023.

Felden, A. M., Martin, D. F., and Ng, E. G.: SUHMO: An Adaptive Mesh Refinement SUbglacial Hydrology MOdel v1.0, Geoscientific Model Development, 16, 407–425, https://doi.org/10.5194/gmd-16-407-2023, 2023.

Flowers, G. E.: Modelling Water Flow under Glaciers and Ice Sheets, Proceedings of the Royal Society of London A: Mathematical, Physical and Engineering Sciences, 471, 20140 907, https://doi.org/10.1098/rspa.2014.0907, 2015.

Flowers, G. E. and Clarke, G. K. C.: A Multicomponent Coupled Model of Glacier Hydrology 1. Theory and Synthetic Examples, Journal of Geophysical Research: Solid Earth, 107, ECV 9–1–ECV 9–17, https://doi.org/10.1029/2001JB001122, 2002.

Gagliardini, O. and Werder, M. A.: Influence of Increasing Surface Melt over Decadal Timescales on Land-Terminating Greenland-type Outlet Glaciers, Journal of Glaciology, 64, 700–710, https://doi.org/10.1017/jog.2018.59, 2018.

Gimbert, F., Tsai, V. C., Amundson, J. M., Bartholomaus, T. C., and Walter, J. I.: Subseasonal Changes Observed in Subglacial Channel Pressure, Size, and Sediment Transport, Geophysical Research Letters, 43, 3786–3794, https://doi.org/10.1002/2016GL068337, 2016.

Goldberg, D. N.: A Variationally Derived, Depth-Integrated Approximation to a Higher-Order Glaciological Flow Model, Journal of Glaciology, 57, 157–170, https://doi.org/10.3189/002214311795306763, 2011.

Gray, L., Joughin, I., Tulaczyk, S., Spikes, V. B., Bindschadler, R., and Jezek, K.: Evidence for Subglacial Water Transport in the West Antarctic Ice Sheet through Three-Dimensional Satellite Radar Interferometry, Geophysical Research Letters, 32, L03 501, https://doi.org/10.1029/2004GL021387, 2005.

Hewitt, I. J.: Modelling Distributed and Channelized Subglacial Drainage: The Spacing of Channels, Journal of Glaciology, 57, 302–314, https://doi.org/10.3189/002214311796405951, 2011.

Hewitt, I. J.: Seasonal Changes in Ice Sheet Motion Due to Melt Water Lubrication, Earth and Planetary Science Letters, 371–372, 16–25, https://doi.org/10.1016/j.epsl.2013.04.022, 2013.

Hewitt, I. J., Schoof, C., and Werder, M. A.: Flotation and Free Surface Flow in a Model for Subglacial Drainage. Part II: Channel Flow, Journal of Fluid Mechanics, 702, 157–187, https://doi.org/10.1017/jfm.2012.166, 2012.

Hill, T., Flowers, G. E., Hoffman, M. J., Bingham, D., and Werder, M. A.: Improved Representation of Laminar and Turbulent Sheet Flow in Subglacial Drainage Models, Journal of Glaciology, pp. 1–14, https://doi.org/10.1017/jog.2023.103, 2023.

Hooke, R. L.: On the Role of Mechanical Energy in Maintaining Subglacial Water Conduits at Atmospheric Pressure, Journal of Glaciology, 30, 180–187, 1984.

Huss, M., Bauder, A., Werder, M., Funk, M., and Hock, R.: Glacier-Dammed Lake Outburst Events of Gornersee, Switzerland, Journal of Glaciology, 53, 189–200, https://doi.org/10.3189/172756507782202784, 2007.

Iken, A., Röthlisberger, H., Flotron, A., and Haeberli, W.: The Uplift of Unteraargletscher at the Beginning of the Melt Season—A Consequence of Water Storage at the Bed?, Journal of Glaciology, 29, 28–47, https://doi.org/10.3189/S0022143000005128, 1983.

Irarrazaval, I., Werder, M. A., Linde, N., Irving, J., Herman, F., and Mariethoz, G.: Bayesian Inference of Subglacial Channel Structures from Water Pressure and Tracer-Transit Time Data: A Numerical Study Based on a 2-D Geostatistical Modeling Approach, Journal of Geophysical Research: Earth Surface, 124, 1625–1644, https://doi.org/10.1029/2018JF004921, 2019.

Irarrazaval, I., Werder, M. A., Huss, M., Herman, F., and Mariethoz, G.: Determining the Evolution of an Alpine Glacier Drainage System by Solving Inverse Problems, Journal of Glaciology, 67, 421–434, https://doi.org/10.1017/jog.2020.116, 2021.

https://doi.org/10.5194/egusphere-2026-4310
Preprint. Discussion started: 28 July 2026

Kamb, B.: Glacier Surge Mechanism Based on Linked Cavity Configuration of the Basal Water Conduit System, Journal of Geophysical Research, 92, 9083–9099, https://doi.org/10.1029/JB092iB09p09083, 1987.

Kamb, B. and Engelhardt, H.: Waves of Accelerated Motion in a Glacier Approaching Surge: The Mini-Surges of Variegated Glacier, Alaska, U.S.A., Journal of Glaciology, 33, 27–46, https://doi.org/10.3189/S0022143000005311, 1987.

Kazmierczak, E., Gregov, T., Coulon, V., and Pattyn, F.: A Fast and Simplified Subglacial Hydrological Model for the Antarctic Ice Sheet and Outlet Glaciers, The Cryosphere, 18, 5887–5911, https://doi.org/10.5194/tc-18-5887-2024, 2024.

Lai, C.-Y., Stevens, L. A., Chase, D. L., Creyts, T. T., Behn, M. D., Das, S. B., and Stone, H. A.: Hydraulic Transmissivity Inferred from Ice-Sheet Relaxation Following Greenland Supraglacial Lake Drainages, Nature Communications, 12, 3955, https://doi.org/10.1038/s41467-021-24186-6, 2021.

Maier, N., Andersen, J. K., Mouginot, J., Gimbert, F., and Gagliardini, O.: Wintertime Supraglacial Lake Drainage Cascade Triggers Large-Scale Ice Flow Response in Greenland, Geophysical Research Letters, 50, e2022GL102 251, https://doi.org/10.1029/2022GL102251, 2023.

Maranzoni, A., Dazzi, S., Aureli, F., and Mignosa, P.: Extension and Application of the Preissmann Slot Model to 2D Transient Mixed Flows, Advances in Water Resources, 82, 70–82, https://doi.org/10.1016/j.advwatres.2015.04.010, 2015.

McArthur, K., McCormack, F. S., and Dow, C. F.: Basal Conditions of Denman Glacier from Glacier Hydrology and Ice Dynamics Modeling, The Cryosphere, 17, 4705–4727, https://doi.org/10.5194/tc-17-4705-2023, 2023.

Mejia, J. Z., Gulley, J. D., Trunz, C., Covington, M. D., Bartholomaus, T. C., Xie, S., and Dixon, T. H.: Isolated Cavities Dominate Greenland Ice Sheet Dynamic Response to Lake Drainage, Geophysical Research Letters, 48, e2021GL094 762, https://doi.org/10.1029/2021GL094762, 2021.

Morlighem, M., Rignot, E., Binder, T., Blankenship, D., Drews, R., Eagles, G., Eisen, O., Ferraccioli, F., Forsberg, R., Fretwell, P., Goel, V., Greenbaum, J. S., Gudmundsson, H., Guo, J., Helm, V., Hofstede, C., Howat, I., Humbert, A., Jokat, W., Karlsson, N. B., Lee, W. S., Matsuoka, K., Millan, R., Mouginot, J., Paden, J., Pattyn, F., Roberts, J., Rosier, S., Ruppel, A., Seroussi, H., Smith, E. C., Steinhage, D., Sun, B., van den Broeke, M. R., van Ommen, T. D., van Wessem, M., and Young, D. A.: Deep Glacial Troughs and Stabilizing Ridges Unveiled beneath the Margins of the Antarctic Ice Sheet, Nature Geoscience, 13, 132–137, https://doi.org/10.1038/s41561-019-0510-8, 2020.

Morlighem, M., Williams, C., Rignot, E., An, L., Arndt, J. E., Bamber, J., Catania, G., Chauché, N., Dowdeswell, J. A., Dorschel, B., Fenty, I., Hogan, K., Howat, I., Hubbard, A., Jakobsson, M., Jordan, T. M., Kjeldsen, K. K., Millan, R., Mayer, L., Mouginot, J., Noël, B., O'Cofaigh, C., Palmer, S. J., Rysgaard, S., Seroussi, H., Siegert, M. J., Slabon, P., Straneo, F., van den Broeke, M. R., Weinrebe, W., Wood, M., and Zinglersen, K.: IceBridge BedMachine Greenland (IDBMG4, Version 6), https://doi.org/10.5067/6B6B225B8V2D, 2025.

Nienow, P. W., Sharp, M., and Willis, I. C.: Velocity-Discharge Relationships Derived from Dye Tracer Experiments in Glacial Meltwaters: Implications for Subglacial Flow Conditions, Hydrological Processes, 10, 1411–1426, 1996.

Nye, J. F.: Water Flow in Glaciers: Jökulhlaups, Tunnels and Veins, Journal of Glaciology, 17, 181–207, https://doi.org/10.3189/S002214300001354X, 1976.

Preissmann, A. and Cunge, J. A.: Calcul Du Mascaret Sur Machine Électronique, La Houille Blanche, 47, 588–596, https://doi.org/10.1051/lhb/1961045, 1961.

Riesen, P., Sugiyama, S., and Funk, M.: The Influence of the Presence and Drainage of an Ice-Marginal Lake on the Ice Flow of Gornergletscher, Switzerland, Journal of Glaciology, 56, 278–286, https://doi.org/10.3189/002214310791968575, 2010.

https://doi.org/10.5194/egusphere-2026-4310
Preprint. Discussion started: 28 July 2026

Röthlisberger, H.: Water Pressure in Intra– and Subglacial Channels, Journal of Glaciology, 11, 177–203, https://doi.org/10.3189/S0022143000022188, 1972.

Scholzen, C., Schuler, T. V., and Gilbert, A.: Sensitivity of Subglacial Drainage to Water Supply Distribution at the Kongsfjord Basin, Svalbard, The Cryosphere, 15, 2719–2738, https://doi.org/10.5194/tc-15-2719-2021, 2021.

Schoof, C.: Ice-Sheet Acceleration Driven by Melt Supply Variability, Nature, 468, 803–806, https://doi.org/10.1038/nature09618, 2010.

Schoof, C., Hewitt, I. J., and Werder, M. A.: Flotation and Free Surface Flow in a Model for Subglacial Drainage. Part I: Distributed Drainage, Journal of Fluid Mechanics, 702, 126–156, https://doi.org/10.1017/jfm.2012.165, 2012.

Schuler, T. V. and Fischer, U. H.: Modeling the Diurnal Variation of Tracer Transit Velocity through a Subglacial Channel, Journal of Geophysical Research, 114, https://doi.org/10.1029/2008JF001238, 2009.

Seaberg, S. Z., Seaberg, J. Z., Hooke, R. L., and Wiberg, D. W.: Character of the Englacial and Subglacial Drainage System in the Lower Part of the Ablation Area of Storglaciären, Sweden, as Revealed by Dye-Trace Studies, Journal of Glaciology, 34, 217–227, https://doi.org/10.3189/S0022143000032263, 1988.

Sole, A. J., Mair, D. W. F., Nienow, P. W., Bartholomew, I. D., King, M. A., Burke, M. J., and Joughin, I.: Seasonal Speedup of a Greenland Marine-Terminating Outlet Glacier Forced by Surface Melt–Induced Changes in Subglacial Hydrology, Journal of Geophysical Research, 116, F03 014, https://doi.org/10.1029/2010JF001948, 2011.

Sommers, A., Rajaram, H., and Morlighem, M.: SHAKTI: Subglacial Hydrology and Kinetic, Transient Interactions v1.0, Geoscientific Model Development, 11, 2955–2974, https://doi.org/10.5194/gmd-11-2955-2018, 2018.

Stearns, L. A., Smith, B. E., and Hamilton, G. S.: Increased Flow Speed on a Large East Antarctic Outlet Glacier Caused by Subglacial Floods, Nature Geoscience, 1, 827–831, https://doi.org/10.1038/ngeo356, 2008.

Stevens, L. A., Behn, M. D., McGuire, J. J., Das, S. B., Joughin, I., Herring, T., Shean, D. E., and King, M. A.: Greenland Supraglacial Lake Drainages Triggered by Hydrologically Induced Basal Slip, Nature, 522, 73–76, https://doi.org/10.1038/nature14480, 2015.

Stevens, L. A., Hewitt, I. J., Das, S. B., and Behn, M. D.: Relationship Between Greenland Ice Sheet Surface Speed and Modeled Effective Pressure, Journal of Geophysical Research: Earth Surface, 123, 2258–2278, https://doi.org/10.1029/2017JF004581, 2018.

Stevens, L. A., Nettles, M., Davis, J. L., Creyts, T. T., Kingslake, J., Hewitt, I. J., and Stubblefield, A.: Tidewater-Glacier Response to Supraglacial Lake Drainage, Nature Communications, 13, 6065, https://doi.org/10.1038/s41467-022-33763-2, 2022.

Stevens, L. A., Das, S. B., Behn, M. D., McGuire, J. J., Lai, C.-Y., Joughin, I., Larochelle, S., and Nettles, M.: Elastic Stress Coupling Between Supraglacial Lakes, Journal of Geophysical Research: Earth Surface, 129, e2023JF007 481, https://doi.org/10.1029/2023JF007481, 2024.

Sundal, A. V., Shepherd, A., Nienow, P., Hanna, E., Palmer, S., and Huybrechts, P.: Melt-Induced Speed-up of Greenland Ice Sheet Offset by Efficient Subglacial Drainage, Nature, 469, 521–524, https://doi.org/10.1038/nature09740, 2011.

Tsai, V. C. and Rice, J. R.: A Model for Turbulent Hydraulic Fracture and Application to Crack Propagation at Glacier Beds, Journal of Geophysical Research, 115, F03 007, https://doi.org/10.1029/2009JF001474, 2010.

Verjans, V. and Robel, A.: Accelerating Subglacial Hydrology for Ice Sheet Models With Deep Learning Methods, Geophysical Research Letters, 51, e2023GL105 281, https://doi.org/10.1029/2023GL105281, 2024.

Walder, J. S.: Hydraulics of Subglacial Cavities, Journal of Glaciology, 32, 439–445, https://doi.org/10.3189/S0022143000012156, 1986.

Werder, M. A., Hewitt, I. J., Schoof, C. G., and Flowers, G. E.: Modeling Channelized and Distributed Subglacial Drainage in Two Dimensions, Journal of Geophysical Research: Earth Surface, 118, 2140–2158, https://doi.org/10.1002/jgrf.20146, 2013.

Zhang, H., Stevens, L. A., Hewitt, I. J., and Stuart, H.: A Unified Blister and Subglacial Hydrology Framework for Supraglacial Lake Drainage Events, https://doi.org/10.48550/ARXIV.2511.18018, 2025.

https://doi.org/10.5194/egusphere-2026-4310
Preprint. Discussion started: 28 July 2026

Zhao, C., Gladstone, R., Zwinger, T., Gillet-Chaulet, F., Wang, Y., Caillet, J., Mathiot, P., Saraste, L., Jager, E., Galton-Fenzi, B. K., Christoffersen, P., and King, M. A.: Subglacial Water Amplifies Antarctic Contributions to Sea-Level Rise, Nature Communications, 16, 3187, https://doi.org/10.1038/s41467-025-58375-4, 2025.